13. Kelso, J. A. S., Buchanan, J. J. & Wallace, S. A. Order parameters for the neural organization of single, multijoint limb movement patterns. *Exp. Brain Res.* **85,** 432–444 (1991).
14. Riek, S., Carson, R. G. & Byblow, W. D. Spatial and muscular dependencies in bimanual coordination. *J. Hum. Mov. Stud.* **23,** 251–265 (1992).
15. Scholz, J. P. & Kelso, J. A. S. A quantitative approach to understanding the formation and change of coordinated movement patterns. *J. Mot. Behav.* **21,** 122–144 (1989).
16. Carson, R. G. The dynamics of isometric bimanual coordination. *Exp. Brain Res.* **105,** 465–476 (1995).
17. Cattaert, D., Semjen, A. & Summers, J. J. Simulating a neural cross-talk model for between-hand interference during bimanual circle drawing. *Biol. Cybern.* **81,** 343–358 (1999).
18. Heuer, H. Structural constraints on bimanual movements. *Psychol. Res.* **55,** 83–98 (1993).
19. Semjen, A., Summers, J. J. & Cattaert, D. The coordination of the hands in bimanual circle drawing. *J. Exp. Psychol. Hum. Percept.* **21,** 1139–1157 (1995).
20. Carson, R. G., Thomas, J., Summers, J. J., Walters, M. R. & Semjen, A. The dynamics of bimanual circle drawing. *Q. J. Exp. Psychol.* **50A,** 664–683 (1997).
21. Sternad, D. Debates in dynamics: a dynamical systems perspective on action and perception. *Hum. Mov. Sci* **19,** 407–423 (2000).
22. Riley, M. A. & Turvey, M. T. Dynamics in action: intentional behavior as a complex system. *Am. J. Psychol.* **114,** 160–169 (2001).
23. Park, H., Collins, D. R. & Turvey, M. T. Dissociation of muscular and spatial constraints on patterns of interlimb coordination. *J. Exp. Psychol. Hum.* **27,** 32–47 (2001).
24. Saltzman, E. L. in *Mind as Motion. Explorations in the Dynamics of Cognition* (eds Port, R. F. & van Gelder, T.) 149–173 (MIT Press, Cambridge, 1995).
25. Amazeen, P. G., Amazeen, E. L. & Turvey, M. T. Breaking the reflectional symmetry of interlimb coordination dynamics. *J. Mot. Behav.* **30** (3), 199–216 (1998).
26. Zaal, F. T. J. M., Bingham, G. P. & Schmidt, R. C. Visual perception of mean relative phase and phase variability. *J. Exp. Psychol. Hum. Percept.* **26,** 1209–1220 (2000).
27. Schmidt, R. A. in *Human Motor Behavior: An Introduction* (ed. Kelso, J. A. S.) 189–235 (Erlbaum, Hillsdale, New Jersey, 1982).
28. Jordan, M. I. in *The Cognitive Neurosciences* (ed. Gazzaniga, M. S.) 597–609 (MIT Press, Cambridge, 1995).
29. Wolpert, D. M. & Ghahramani, Z. Computational principles of movement neuroscience. *Nature Neurosci.* (Suppl.) **3,** 1212–1217 (2000).
30. Prinz, W. Perception and action planning. *Europ. J. Cogn. Psychol.* **9** (20), 129–154 (1997).

Acknowledgements

We wish to thank S. Jordan for discussions; F. Banci for constructing the apparatus used in experiment 3; S. Alessio, B. Schroer and M. Hove for running the experiments; and S. Hass for suggestions concerning the experimental procedure.

Correspondence and requests for materials should be addressed to F.M. (e-mail: mechsner@mpipf-muenchen.mpg.de).

Energetics of ion conduction through the K^+ channel

Simon Bernèche & Benoît Roux

Department of Biochemistry, Weill Medical College of Cornell University, 1300 York Avenue, New York, New York 10021, USA; Département de Physique, Université de Montréal, Montréal, Québec H3C 3J7, Canada

K^+ channels are transmembrane proteins that are essential for the transmission of nerve impulses. The ability of these proteins to conduct K^+ ions at levels near the limit of diffusion is traditionally described in terms of concerted mechanisms in which ion-channel attraction and ion–ion repulsion have compensating effects, as several ions are moving simultaneously in single file through the narrow pore[1–4]. The efficiency of such a mechanism, however, relies on a delicate energy balance—the strong ion-channel attraction must be perfectly counterbalanced by the electrostatic ion–ion repulsion. To elucidate the mechanism of ion conduction at the atomic level, we performed molecular dynamics free energy simulations on the basis of the X-ray structure of the KcsA K^+ channel[4]. Here we find that ion conduction involves transitions between two main states, with two and three K^+ ions occupying the selectivity filter, respectively; this process is reminiscent of the 'knock-on' mechanism proposed by Hodgkin and Keynes in 1955[1]. The largest free energy barrier is on the order of 2–3 kcal mol^{-1}, implying that the process of ion conduction is limited by diffusion. Ion–ion repulsion, although essential for rapid conduction, is shown to act only at very short distances. The calculations show also that the rapidly conducting pore is selective.

The crystallographic structure of the KcsA K^+ channel revealed that the pore comprises a wide, nonpolar cavity of 8 Å radius on the intracellular side, leading up on the extracellular side to a narrow pore of 12 Å that is lined exclusively by main chain carbonyl oxygens[4]. This region of the pore acts as a 'selectivity filter' by allowing only the passage of K^+ ions across the cell membrane[4], whereas the wide cavity helps overcome the dielectric barrier caused by the cell membrane[5]. The translocation of K^+ ions in single file through the narrowest region of the pore is expected to be the rate-limiting step in the conduction mechanism. This process can be represented schematically:

$$K^+ \quad \overline{K^+ \; K^+} \quad \rightleftharpoons \quad \overline{K^+ \; K^+} \quad K^+ \qquad (1)$$

in which the approach of one ion from one side of the selectivity filter is coupled to the simultaneous exit of an other ion on the opposite side. Although such a concerted mechanism is consistent with long-held views of ion conduction through K^+ channels[1–4], how it takes place at the atomic level remains unresolved. A simple calculation shows that the direct ion–ion repulsion varies by tens of kcal mol^{-1} when two or three ions are in the pore. Somehow, the K^+ channel is able to exploit such large energies in a productive manner to yield a flux of about 10^8 ions s^{-1}. This implies that there is no significant activation free energy barrier opposing the concerted ion translocation. How can this be possible?

Although the available experimental data provide a wealth of information about the structure and function of K^+ channels, theoretical considerations are necessary for understanding the energetics of ion conduction at the atomic level. One approach to refine our understanding of complex biomolecular systems is to use

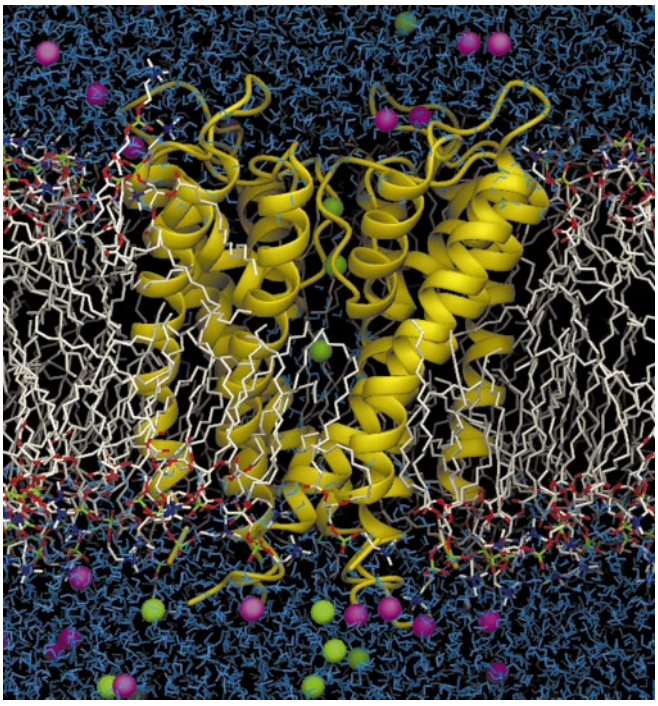

Figure 1 Molecular representation of the atomic model of the KcsA K^+ channel embedded in an explicit DPPC phosphilipid membrane bathed by a 150 mM KCl aqueous salt solution[11].

molecular dynamics simulations[6]. However, straight molecular dynamics trajectories of KcsA (although informative) remain limited because the average time required for the permeation of a single ion is typically much longer than can be simulated currently[7–11]. To circumvent these difficulties and characterize the mechanism of ion conduction quantitatively, we have computed the multi-ion free energy profile governing the elementary microscopic steps of ion translocation in the pore. The free energy profile or potential of mean force (PMF)[12] is the dominant factor governing the mechanism of ion conduction[13]. The free energy surface for ion conduction was calculated using umbrella sampling simulations[14], a powerful computational approach to characterize complex biomolecular systems quantitatively. The simulation system is shown in Fig. 1. First, molecular dynamics simulations are performed in the presence of an artificial biasing potential between the ions and the selectivity filter to obtain a better sampling of the relevant configurations of the system. Next, the bias introduced by this potential is rigorously removed after analysis to characterize the unbiased free energy surface of the system.

The results of the calculations are shown in Fig. 2. To aid visualization the results are presented as two-dimensional topographic maps of the free energy landscape governing the ion conduction through the selectivity filter of the K^+ channel. To produce the two-dimensional maps, the full free energy function $W(Z_1, Z_2, Z_3)$, which depends on the position of the three ions along the channel axis, has been projected onto two different planes with reduced reaction coordinates—the ions are numbered from 1 to 3 starting from the extracellular side. In the first free energy map (Fig. 2, left), the reduced PMF is shown as a function of the position of the ion in the cavity, Z_3, and the position of the centre-of-mass of the two ions in the selectivity filter, Z_{12}. In the second free energy map (Fig. 2, right), the reduced PMF is shown as a function of the position of the outermost ion near the extracellular end of the pore, Z_1, and the position of the centre-of-mass of the two ions in the selectivity filter, Z_{23} (see Methods for further details). Using such reduced reaction coordinates is meaningful because the motions of two ions located in the narrow selectivity filter are highly correlated[11]. Typical configuration of the selectivity filter with the three K^+ permeating ions and nearby water molecules (*a*–*f*) are also given in Fig. 2 to show the elementary steps of ion conduction. Figure 2, with the two-dimensional maps and the associated configurations (*a*–*f*), provides essentially the information connecting the left and right sides of Scheme 1 at the atomic level.

As seen in Fig. 2, the conduction process involves transitions between two main states with two (*a*, *c*, *e*, *f*) or three (*b*, *d*) K^+ ions, respectively, in the selectivity filter. The ions proceed along the pore axis in a single-file fashion with a single water molecule between them, indicating that each permeating K^+ ion is accompanied by about one water molecule in accord with streaming potential measurements[15]. The pathway with the lowest free energy barrier follows the sequence of configurations *a*–*b*–*d*–*f* (dotted line in the two-dimensional maps). Although all the microscopic elementary steps can occur reversibly, we describe and discuss the elementary steps leading to the outward movement of one ion for the sake of clarity. Along this optimal pathway, the ion in the cavity first approaches the intracellular entrance to the selectivity filter (*a*–*b*), then pushes the two ions in the selectivity filter (*b*–*d*) leading to the exit of the outermost ion on the extracellular side (*d*–*e*–*f*). These

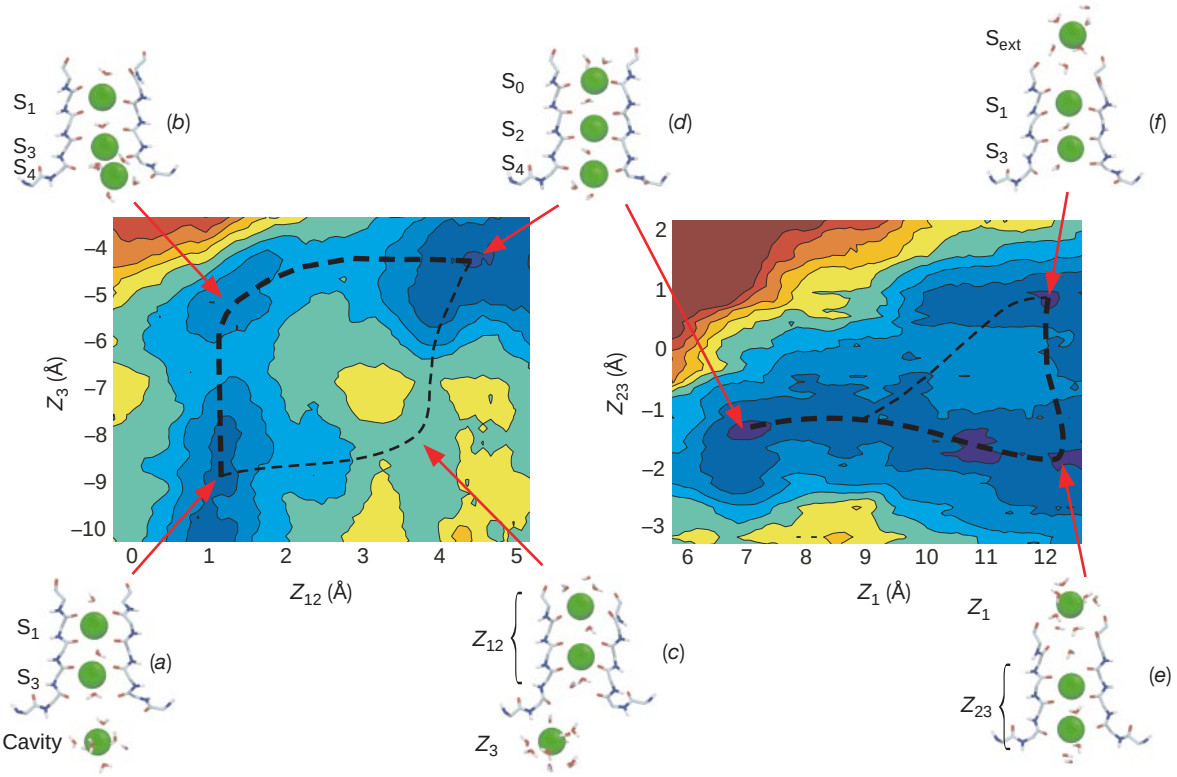

Figure 2 Topographic free energy maps of ion conduction calculated from umbrella sampling molecular dynamics simulations. Each colour level corresponds to an energy of 1 kcal mol^{-1}; the axes are in Å. The position of the ions, Z_1, Z_2 and Z_3 (numbered in successive order starting from the outermost ion) are defined relative to the centre-of-mass of the backbone atoms of residues Thr 75-Val 76-Gly 77-Tyr 78, which constitute the KcsA central core of the selectivity filter. The definition of the reduced reaction coordinates (Z_{12}, Z_3) and (Z_1, Z_{23}) is indicated in *c* and *e*, with Z_{ij} corresponding to the center of mass of ions *i* and *j*. The two-dimensional maps were calculated from a projection of the full three-dimensional PMF and a direct comparison of the energy levels in the two two-dimensional maps is thus meaningful. The lowest energy pathway (highlighted by a dotted line) follows the configurations *a*–*b*–*d*–*f* (a spontaneous transition along this pathway has been observed previously during an unbiased molecular dynamics simulation[11]). A secondary pathway (highlighted by a thin dash line) following the configurations *a*–*c*–*d*–*f* is also possible.

elementary steps are reminiscent of the knock-on mechanism that was proposed nearly 50 years ago[1]. The largest free energy barrier for this process is on the order of 2–3 kcal mol^{-1}, which is remarkable given the very large hydration energies of K^+ ions. Once the outermost ion has exited on the extracellular side ($Z_1 \geq 12$ Å; Fig. 2, right two-dimensional map) the two ions remaining in the selectivity filter can move back and forth in the selectivity filter with a small barrier of approximately 1 kcal mol^{-1} (*e* and *f*), recovering rapidly a productive configuration for conduction. The absence of any significant activation free energy barrier opposing the concerted ion translocation implies that ion conduction is essentially diffusion limited. A second pathway characteristic of a 'vacancy-diffusion' mechanism[16] is also possible (sequence of configurations *a*–*c*–*d*, indicated with a thin, dashed line in Fig. 2). The two ions in the selectivity filter move first (*a*–*c*), leaving a vacant binding site formed by the carbonyl oxygens of Thr 75, which is subsequently occupied by the incoming ion from the cavity (*c*–*d*). The largest energy barriers for this process are on the order of 3–4 kcal mol^{-1}. The existence of multiple pathways may contribute to yielding a high throughput as ion translocation does not have to proceed in a unique fashion.

Even though no large free energy barrier opposing ion conduction is observed in the free energy maps, some positions along the permeation pathway are preferably occupied by K^+ ions. These 'binding sites' are illustrated in Fig. 3 by showing a superposition of a few dynamical configurations associated with the free energy minima in the two dimensional maps. Five specific sites in the selectivity filter are revealed by the superposition. As expected, the sites (S_1–S_4), which were detected in the X-ray structure of KcsA, are observed[4]. Moreover, the calculations reveal the presence of two additional K^+-binding sites, located on the extracellular side of the channel, S_0 and S_{ext}. The K^+ ion in site S_0 is hydrated by 3–4 water molecules and makes some contacts with the carbonyl of Tyr 78, whereas the ion in the outermost site, S_{ext}, is almost fully hydrated. These two binding sites were not detected in the crystallographic structure of KcsA[4], but are now observed in recent diffraction data at higher resolution (R. MacKinnon and J. Cabral, personal communication). Sites S_0, S_2 and S_4 can be occupied simultaneously by K^+ with a single water molecule located between each ion pair, for a total of three K^+ ions in the selectivity filter (Fig. 2d). According to the free energy map shown in Fig. 2, such a configuration K-W-K-W-K corresponds to a shallow free energy well and does not oppose rapid conduction. Recent calculations have indicated that tetraethylammonium (TEA), a well known external blocker of K^+ channels[17], binds favourably in site S_0 in a K-W-K-W-TEA configuration[18].

The details of the process of ion conduction challenge a naive view of repulsive forces in multi-ion transport systems. A particularly notable example is provided by configuration *b* in Fig. 2, in which one ion occupies the inner site S_4 while the other ion occupies the adjacent site S_3. The two ions, which are only 4 Å away from each other, appear to be stabilized by interacting simultaneously with the carbonyl groups of Thr 75. At such a distance the electrostatic energy is +83 kcal mol^{-1}, and the mutual repulsive coulombic force between the two K^+ ions corresponds to an electric field of 9×10^9 V m^{-1}, which is equivalent to the field produced by a transmembrane potential of 27 V. However, the free energy of this configuration is only approximately 1 kcal mol^{-1} higher than the reference configuration *a* according to the two-dimensional map in Fig. 2. Nonetheless, further analysis reveals that repulsive forces are absolutely essential for rapid conduction. Figure 4 shows the free energy profile as a function of the position of the outermost ion

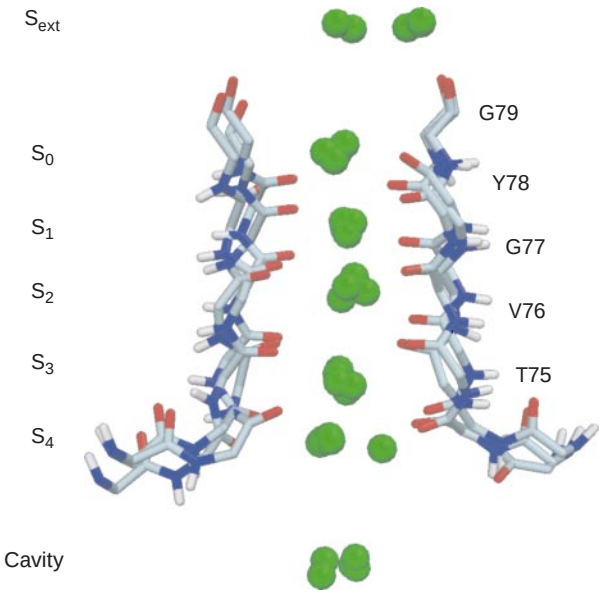

Figure 3 Superposition of instantaneous dynamical configurations showing the dominant ion positions associated with the free energy minima in Fig. 2. The outer site (S_1), the upper inner site (S_3), the lower inner site (S_4) and the diffuse cavity site detected in the initial X-ray structure are shown[4]. Furthermore, K^+ can occupy the site where a crystallographic water was previously detected (S_2), as well as two additional sites termed S_0 and S_{ext}. The ions in S_1, S_2 and S_3 are in contact with the main chain carbonyl oxygens (S_1, Gly 77 and Tyr 78; S_2, Val 76 and Gly 77; S_3, Thr 75 and Val 76) and only 1–2 water molecules, whereas the ion in S_4 is hydrated by 2–3 water molecules and makes intermittent contacts with the carbonyl oxygens and the side chain of Thr 75. The ion in S_0 is in contact with Tyr 78 and is hydrated by 3–4 water molecules. The ion in S_{ext} is almost fully hydrated.

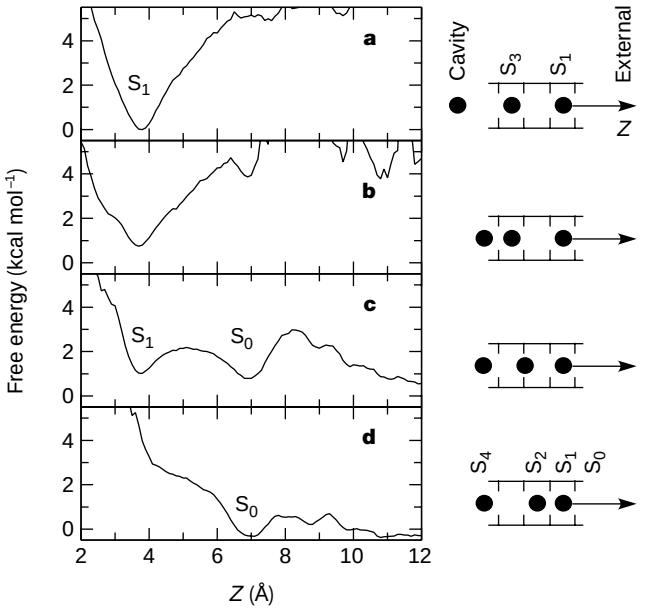

Figure 4 Importance of ion–ion repulsion on the elementary steps of ion conduction. The total free energy of the three-ion system is plotted as a function of the outermost K^+ ion while the two other K^+ ions are fixed at different position in the pore. The corresponding ion configurations of the system are shown schematically on the right. The profiles were extracted from the full three-dimensional free energy $W(Z_1, Z_2, Z_3)$ and the absolute energy scale was preserved (a direct comparison of the profiles is meaningful). **a**, A large free energy barrier prevents the exit of the outer K^+ ion towards the extracellular side as the two other ions are in the cavity and in the inner site (S_3). **b**, **c**, The barrier towards the extracellular side is progressively reduced and site S_0 is slightly stabilized as the cavity ion approaches site S_4 and the other ion initiates a transition from site S_3 to S_2. **d**, Once two ions occupy sites S_4 and S_2, the energy well at site S_1 disappears and the outer ion transits to site S_0.

while the two other ions are fixed at different locations in the pore. Initially, while the two other ions are in the cavity and in the inner site S_3, the outer K^+ ion is located in a deep well and cannot exit towards the extracellular side (Fig. 4a). As the ion in the cavity approaches the inner site S_4 and the second ion initiates a transition from site S_3 to S_2, the bottom of the free energy well is lifted up, thereby decreasing the barrier between sites S_1 and S_0 progressively to 1 kcal mol^{-1} (Fig. 4b, c). Ultimately, the site S_1 becomes unstable and the exit of the ion towards the extracellular side becomes barrierless (Fig. 4d). This series of free energy profiles demonstrates that without the repulsion from the other two incoming ions, the outer ion would be trapped in the site S_1 and its exit towards the extracellular side would require a significant activation free energy.

The calculations show that the conduction of K^+ ions is essentially barrierless. We next sought to determine whether the channel remains selective for K^+ ion. Selectivity arises primarily from differences between the free energy of the ion in the channel and in the bulk solution[19]. To address questions about selectivity, we performed molecular dynamics free energy simulations (MD/FES) in which one K^+ is alchemically transformed into a Na^+ at specific locations along the pore axis[20] (see Methods for details). The calculated excess free energy difference relative to the aqueous solution for the outer site (S_1) near the extracellular surface is about +2.8 kcal mol^{-1}. Moving deeper into the pore, the calculated free energy of the subsequent binding site (S_2) rises to +6.6 kcal mol^{-1}, indicating that there is an increase in the selectivity of the channel. The relative selectivity of the 'external lock-in site' detected in Ba^{2+} blockade experiments has been estimated to be around +5.5 kcal mol^{-1} in one particular mammalian K^+ channel[3]. The calculations show that KcsA has both the ability to rapidly conduct K^+ ions and to discriminate against Na^+. It should be emphasized that the magnitude of the dynamical fluctuations of the carbonyl oxygen atoms that form the selectivity filter (visible in the superposition of configurations shown in Fig. 3) is much larger than the difference in the radius of Na^+ and K^+. This shows that selectivity does not arise from simple geometric considerations based on a rigid pore.

Further computational experiments indicate that the fluctuations of the protein structure can have a considerable influence on the free energy profiles and on the selectivity of the channel. Simulations with an artificial restraint distance of 4 Å imposed between the Tyr 78 side chain (from the GYG signature sequence) and its hydrogen-bonding neighbour Trp 68 exhibit a reduction in the fluctuations of the channel, giving rise to a destabilization of the two-ion state relative to the intermediate three-ion state by 2–3 kcal mol^{-1}. The relative stability of the two states is affected because the entropic contribution from the protein to the free energy profile (artificially reduced by the restraints) is larger when two ions are located in the selectivity filter. Moreover, the reduction in fluctuations also modifies the selectivity of the channel by increasing the excess free energy of Na^+ over K^+ in the selectivity filter. Thus, important properties of the pore are coupled to the fluctuations of the hydrogen bond between Tyr 78 and Trp 68, nearly 12 Å away. This may explain how even relatively conservative mutations at positions distant from the pore can markedly affect the conductance of K^+ channels[21]. It is possible that similar, long-range coupling mechanisms in which the free energy surface governing the translocation of ions is modified in response to a perturbation at a large distance (for example, the binding of ATP), may have an important role in the function of ion pumps[22]. □

Methods

Simulations and parameters

All simulations were carried out using the program CHARMM[23]. The total number of atoms in the simulation system is slightly above 40,000 (KcsA, 112 dipalmitoyl phosphatidylcholine (DPPC), 6,532 water molecules, 3 K^+ in the pore, and 12 K^+ and 23 Cl^- in the bulk solution). The side chain of Glu 71 was constructed in a protonated state forming a hydrogen bond with Asp 80. The channel axis is oriented along the Z axis; the centre of the membrane is at $Z = 0$. The simulation methodology has been described previously[11]. Briefly, the electrostatic interactions were computed with no truncation using the particle mesh Ewald (PME) algorithm[24]. The trajectories were generated with a time step of 0.2 fs at constant pressure (1 atm) and temperature (330 K)[25]. We used the PARAM22 potential function for proteins[26], lipids[27] and the TIP3 water potential[28].

The potential function of the ions was calibrated to yield an accurate description of solvation in bulk water and throughout the selectivity filter of the K^+ channel, which is lined by backbone oxygens. The Lennard–Jones (LJ) parameters of the K^+ and Na^+ ions were adjusted to yield the experimental free energy in liquid water (that is, −80 and −101 kcal mol^{-1}), respectively. In addition, the LJ parameters for the cation-carbonyl oxygen pairs were refined to yield solvation free energies in liquid *N*-methylacetamide identical to those in bulk water. The parameters were refined using the spherical solvent boundary potential, which incorporates the long-range electrostatic reaction field[29].

Umbrella sampling PMF and selectivity calculations

For the umbrella sampling PMF calculations, a total of 308 independent simulations of 100 ps with a biasing harmonic potential centred first on Z_{12} and Z_3 (varying successively from 0 to 5.0 and −10.0 to −3.5 every 0.5 Å), and then on Z_1 and Z_{23} (varying successively from 6.0 to 12.5 and −3.0 to 2.0 every 0.5 Å) were generated with a force constant of 20 kcal mol^{-1} Å^{-2}. The centre-of-mass biasing potentials were implemented using the MMFP option of CHARMM[23]. The entire simulation time included in the PMF calculations is nearly 38 ns. The umbrella sampling simulations were unbiased together using the weighted histogram analysis method (WHAM)[30] to calculate the full PMF $W(Z_1, Z_2, Z_3)$. This was then projected onto the reduced reaction coordinates (Z_{12}, Z_3) and (Z_1, Z_{23}) to yield two-dimensional, free energy maps. The projection maintains the relative energy levels shown in the two two-dimensional maps.

For the selectivity calculations, each alchemical free energy difference between K^+ and Na^+ was obtained from forward and backward MD/FES trajectories, generated with the thermodynamic coupling parameter method[20], for a total of 440 ps. The total free energy difference was then calculated using WHAM[30]. Similar calculations have been performed previously using reduced models of the KcsA channel[9,10].

Received 16 August; accepted 8 September 2001.

1. Hodgkin, A. L. & Keynes, R. D. The potassium permeability of a giant nerve fibre. *J. Physiol.* **128,** 61–88 (1955).
2. Hille, B. & Schwarz, W. Potassium channels as multi-ion single-file pores. *J. Gen. Physiol.* **72,** 409–442 (1978).
3. Neyton, J. & Miller, C. Discrete Ba^{2+} block as a probe of ion occupancy and pore structure in the high-conductance Ca^{2+}-activated K^+ channel. *J. Gen. Physiol.* **92,** 569–586 (1988).
4. Doyle, D. A. *et al.* The structure of the potassium channel: molecular basis of K^+ conduction and selectivity. *Science* **280,** 69–77 (1998).
5. Roux, B. & MacKinnon, R. The cavity and pore helices in the KcsA K^+ channel: electrostatic stabilization of monovalent cations. *Science* **285,** 100–102 (1999).
6. Karplus, M. & Petsko, G. A. Molecular dynamics simulations in biology. *Nature* **347,** 631–639 (1990).
7. Guidoni, L., Torre, V. & Carloni, P. Potassium and sodium binding to the outer mouth of the K^+ channel. *Biochem.* **38,** 8599–8604 (1999).
8. Shrivastava, I. H. & Sansom, M. S. Simulations of ion permeation through a potassium channel: molecular dynamics of KcsA in a phospholipid bilayer. *Biophys. J.* **78,** 557–570 (2000).
9. Allen, T. W., Bliznyuk, A., Rendell, A. P., Kuyucak, S. & Chung, S. H. The potassium channel: structure, selectivity and diffusion. *J. Chem. Phys.* **112,** 8191–8204 (2000).
10. Aqvist, J. & Luzhkov, V. Ion permeation mechanism of the potassium channel. *Nature* **404,** 881–884 (2000).
11. Bernèche, S. & Roux, B. Molecular dynamics of the KcsA K(+) channel in a bilayer membrane. *Biophys. J.* **78,** 2900–2917 (2000).
12. Kirkwood, J. G. Statistical mechanics of fluid mixtures. *J. Chem. Phys.* **3,** 300–313 (1935).
13. Roux, B. Statistical mechanical equilibrium theory of selective ion channels. *Biophys. J.* **77,** 139–153 (1999).
14. Torrie, G. M. & Valleau, J. P. Nonphysical sampling distributions in Monte Carlo free-energy estimation: umbrella sampling. *J. Comp. Phys.* **23,** 187–199 (1977).
15. Alcayaga, C., Cecchi, X., Alvarez, O. & Latorre, R. Streaming potential measurements in Ca^{2+}-activated K^+ channels from skeletal and smooth muscle. Coupling of ion and water fluxes. *Biophys. J.* **55,** 367–371 (1989).
16. Schumaker, M. F. & MacKinnon, R. A simple model for multi-ion permeation. single-vacancy conduction in a simple pore model. *Biophys. J.* **58,** 975–984 (1990).
17. Armstrong, C. M. Induced inactivation of the potassium permeability of squid axon membranes. *Nature* **219,** 1262–1263 (1968).
18. Crouzy, S., Berneche, S. & Roux, B. Extracellular blockade of K^+ channels by TEA: results from molecular dynamics simulations of the KcsA channel. *J. Gen. Physiol.* **118,** 207–218 (2001).
19. Eisenman, G. Cation selective electrodes and their mode of operation. *Biophys. J.* **2** (Suppl. 2), 259–323 (1962).
20. Kollman, P. A. Free energy calculations: applications to chemical and biochemical phenomena. *Chem. Rev.* **93,** 2395–2417 (1993).
21. Perozo, E., MacKinnon, R., Bezanilla, F. & Stefani, E. Gating currents from a nonconducting mutant reveal open-closed conformations in Shaker K^+ channels. *Neuron* **11,** 353–358 (1993).
22. Lauger, P. A channel mechanism for electrogenic ion pumps. *Biochim. Biophys. Acta* **552,** 143–161 (1979).
23. Brooks, B. R. *et al.* CHARMM: a program for macromolecular energy minimization and dynamics calculations. *J. Comput. Chem.* **4,** 187–217 (1983).
24. Essmann, U. *et al.* A smooth particle mesh Ewald method. *J. Chem. Phys.* **103,** 8577–8593 (1995).
25. Feller, S. E., Zhang, Y. H., Pastor, R. W. & Brooks, B. R. Constant pressure molecular dynamics simulation—the Langevin piston method. *J. Chem. Phys.* **103,** 4613–4621 (1995).

26. MacKerell, A. D. Jr *et al.* All-atom empirical potential for molecular modeling and dynamics studies of proteins. *J. Phys. Chem. B* **102,** 3586–3616 (1998).
27. Schlenkrich, M. J., Brickmann, J., MacKerell, A. D. Jr & Karplus, M. in *Biological Membranes. A Molecular Perspective from Computation and Experiment* (eds Merz, K. M. & Roux, B.) 31–81 (Birkhauser, Boston, 1996).
28. Jorgensen, W. L., Chandrasekhar, J., Madura, J. D., Impey, R. W. & Klein, M. L. Comparison of simple potential functions for simulating liquid water. *J. Chem. Phys.* **79,** 926–935 (1983).
29. Beglov, D. & Roux, B. Finite representation of an infinite bulk system: solvent boundary potential for computer simulations. *J. Chem. Phys.* **100,** 9050–9063 (1994).
30. Kumar, S., Bouzida, D., Swendsen, R. H., Kollman, P. A. & Rosenberg, J. M. The weighted histogram analysis method for free-energy calculations on biomolecules. I. The method. *J. Comp. Chem.* **13,** 1011–1021 (1992).

Acknowledgements

Discussions with R. MacKinnon and J. Cabral are gratefully acknowledged. This work was supported by the National Institutes of Health and by the Canadian Institutes of Health Research. Several calculations were performed at the RQCHP Computer Center of the University of Montreal and at the National Center for Supercomputing Applications (NCSA) of the University of Illinois at Urbana-Champaign. We are grateful to B. Lorazo for his support. All the molecular pictures were drawn with DINO (A. Philippsen).

Correspondence and requests for materials should be addressed to B.R. (e-mail: benoit.roux@med.cornell.edu).

Maintenance of an unfolded polypeptide by a cognate chaperone in bacterial type III secretion

C. Erec Stebbins* & Jorge E. Galán

Section of Microbial Pathogenesis, Boyer Center for Molecular Medicine, Yale School of Medicine, New Haven, Connecticut 06536, USA

Many bacterial pathogens use a type III protein secretion system to deliver virulence effector proteins directly into the host cell cytosol, where they modulate cellular processes[1,2]. A requirement for the effective translocation of several such effector proteins is the binding of specific cytosolic chaperones, which typically interact with discrete domains in the virulence factors[3,4,5]. We report here the crystal structure at 1.9 Å resolution of the chaperone-binding domain of the *Salmonella* effector protein SptP with its cognate chaperone SicP. The structure reveals that this domain is maintained in an extended, unfolded conformation that is wound around three successive chaperone molecules. Short segments from two different SptP molecules are juxtaposed by the chaperones, where they dimerize across a hydrophobic interface. These results imply that the chaperones associated with the type III secretion system maintain their substrates in a secretion-competent state that is capable of engaging the secretion machinery to travel through the type III apparatus in an unfolded or partially folded manner.

Comprising more than 20 proteins and closely related to the flagellar assembly apparatus, type III systems stand among the most complex protein secretion systems known[1,2]. A distinguishing essential feature of these systems is the requirement of a family of customized cytoplasmic chaperones for the secretion of their cognate substrate effector proteins[3,4,5]. Each chaperone is specific in most cases for one or, in a few cases, two secreted proteins. Therefore, absence of a given chaperone affects the secretion only of its cognate secreted protein, which prematurely degrades or accumulates within the bacterial cytoplasm. Although there is little amino-acid sequence similarity among these chaperones, they share several features such as a comparatively small relative molecular mass (<20,000; M_r <20K), a generally low isoelectric point and a secondary structure predicted to be predominantly helical. The actual function of these chaperones is poorly understood. SptP is a tyrosine phosphatase[6] and GTPase activating protein (GAP) for Cdc42 and Rac[7,8] that reverses the changes induced by *Salmonella* on entry into host cells[9]. SicP is an acidic protein of M_r 14K required for the stability of SptP within the bacterium and its secretion through the type III secretion system[10]. Previous deletion analysis established that SptP residues 15–100 were sufficient to bind SicP[10], but protease footprinting indicates that a different polypeptide segment is protected by the chaperone (Fig. 1a and b). The structure of this protected complex was determined by multiple-wavelength anomalous dispersion (MAD) from the scattering of 31 bromine ions

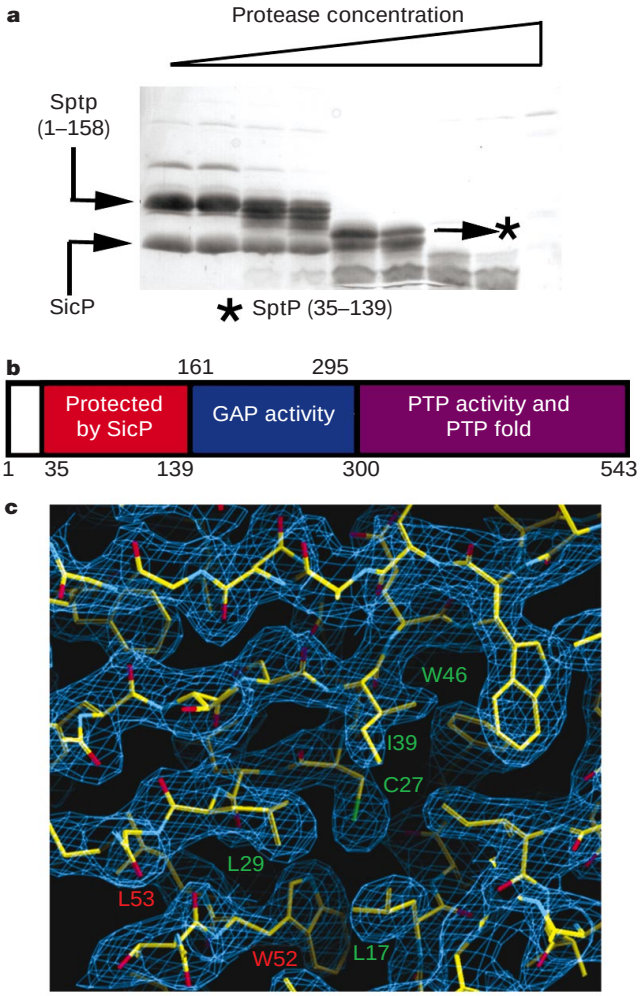

Figure 1 Protease footprinting delineates the chaperone-binding sequence of SptP. **a**, Purified SicP–SptP$^{1-158}$ was incubated on ice for 30 min with increasing concentrations of the protease subtilisin. A fragment of SptP (asterisk) was protected by SicP, and determined by N-terminal sequencing and mass spectroscopy to span SptP residues 35–139. **b**, Domain schematic of SptP. The protected, chaperone-binding domain is shown in red, and the enzymatic effector domains in blue (for the GAP) and purple (for the tyrosine phosphatase domain). The amino-acid numbers that mark the beginning and end of each domain are labelled. **c**, Electron density from a map calculated with MAD solvent-flattened phases to 2.2 Å resolution and contoured at 1.0σ. Residues from the final, refined models of SptP and SicP are shown with atoms of oxygen, nitrogen and carbon in red, blue and yellow, respectively. Some amino-acid side chains around W52 of SptP are labelled in green (SicP) or red (SptP).

* Present address: Laboratory of Structural Microbiology, The Rockefeller University, Box 52, 1230 York Avenue, New York, New York 10021, USA.